

Modeling of a Stewart Platform for Analyzing One Directional Dynamics for Spacecraft Docking Operations

Leonardo Herrera, Shield B. Lin, Stephen J. Montgomery-Smith, Ziraguen O. Williams

Abstract—A one-directional dynamic model of a Stewart Platform was developed to assist NASA in analyzing the dynamic response in spacecraft docking operations. A simplified mechanical drawing was created, capturing the physical structure's main features. A simplified schematic diagram was developed into a lumped mass model from the mechanical drawing. Three differential equations were derived according to the schematic diagram. A Simulink diagram was created using MATLAB to represent the three equations. System parameters, including spring constants and masses, are derived in detail from the physical system. The model can be used for further analysis via computer simulation in predicting dynamic response in its main docking direction, i.e., up-and-down motion.

Keywords—Stewart platform, docking operation, spacecraft, spring constant.

I. INTRODUCTION

THE general figure of a Stewart platform includes a top plate, a bottom plate, and six legs connecting the two plates. All connections between actuators and the baseplate are made of universal joints. Devices placed on the top plate can be moved in six degrees of freedom in which it is possible for a freely-suspended body to move in three linear directions, i.e., lateral, longitudinal, and vertical, and in three rotations, i.e., roll, pitch, and yaw. This specialized layout was first used by V. Eric Gough. The design was later published in a 1965 paper by D. Stewart of the United Kingdom Institution of Mechanical Engineers [1]. Stewart platforms are also known by other names. They are sometimes called a six-axis platform or a six-degree-of-freedom platform. It may also be referred to as a synergistic motion platform due to the mutual interaction between the way that the actuators are programmed.

Hardware simulators have been used to simulate docking operations for spacecraft for the past sixty years. In 1964, Langley Research Center in the USA established a docking simulator [2]. In 1971, the former USSR designed a docking simulator that has been employed to test the APAS-89 docking mechanism [3]. Europe Space Bureau began to research and develop a docking mechanism for unmanned spacecraft in the 1980's. About the same time, Japan developed a docking operation test system in the on-orbit docking of the ETS-7 unmanned spacecraft [4]. China began a manned space program

in the 1990's and developed an integrated testing system for a docking mechanism by the Harbin Institute of Technology and Shanghai Space Bureau in 2000's [5].

NASA Johnson Space Center (JSC) in Houston, Texas, USA built a Stewart Platform in its lab as shown in Fig. 1. It is a parallel manipulator that has six actuators, three pairs attached on its base crossing over to three mounting points on the top plate. With six actuators, the platform can move in six degrees of freedom: back/forward, left/right, up/down, pitch, yaw, and roll. Due to its capabilities, it has many applications on the field with one being docking for spacecraft.

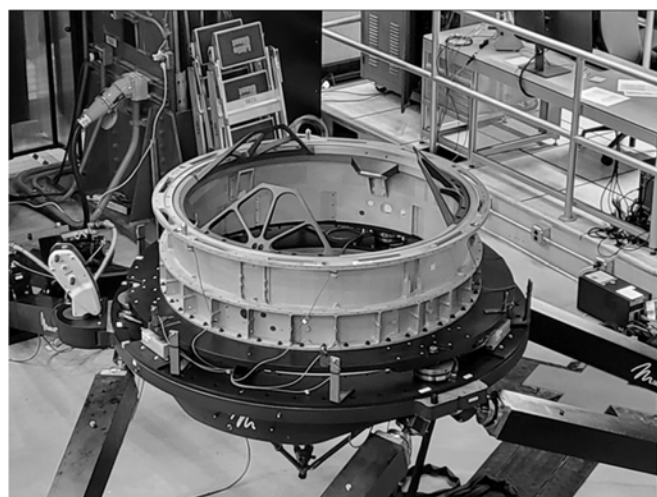


Fig. 1 A Stewart Platform Setup at NASA Johnson Space Center

II. MECHANICAL MODEL OF STEWART PLATFORM

Based on the physical structure of the Stewart Platform, a simplified mechanical drawing was created to capture the main figure along with major masses and joint mechanisms as shown in Fig. 2.

The goal of this task is to derive and study a one directional dynamic motion, in the up-and-down direction, of the Stewart Platform to investigate its response for docking tests. A further simplified schematic diagram is drawn in Fig. 3 to represent the Stewart Platform's motion in the up-and-down direction. A lumped mass model is implemented into the schematic diagram as shown in Fig. 3. Flexible mechanical components were

Leonardo Herrera is with the Department of Mechanical Engineering at Prairie View A&M University, Prairie View, Texas, USA.

Shield B. Lin is with the Department of Mechanical Engineering at Prairie View A&M University, Prairie View, Texas, USA (e-mail: shlin@pvamu.edu).

Stephen J. Montgomery-Smith is with the Department of Mathematics at University of Missouri in Columbia, Missouri, USA.

Ziraguen O. Williams is with CACI International Inc., Houston, Texas, USA.

identified as spring elements and rigid mechanical components were identified as masses provided. The components carry significant quantities of mass. For those spring elements which have non-negligible masses, since not all of the spring's length moves at the same velocity, its kinetic energy is not equal to $\frac{1}{2}mv^2$. As such, m cannot be simply added to the adjacent mass to determine the dynamic behavior. An effective mass of the spring element is calculated that needs to be added to the adjacent mass to correctly predict the behavior of the system [6].



Fig. 2 Simplified Stewart Platform Mechanical Drawing

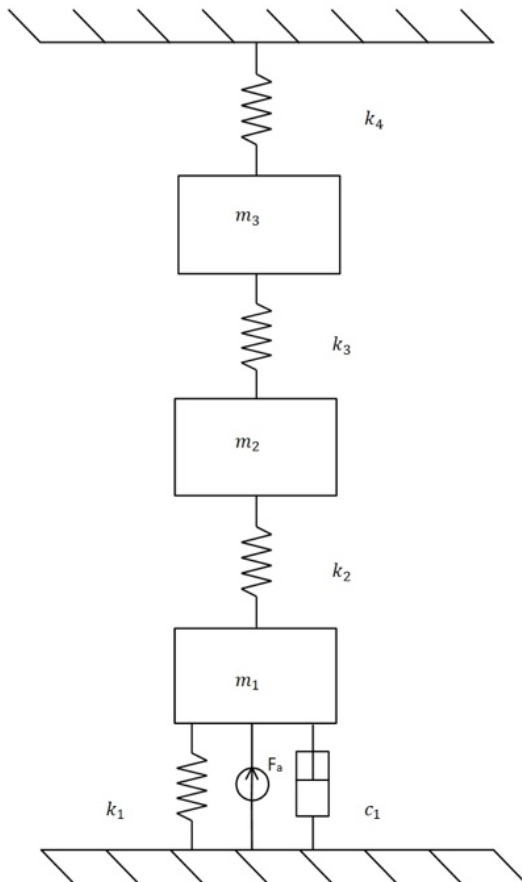


Fig. 3 Schematic Diagram of Lumped Mass Model

Fig. 4 summarizes the definitions of the parameters used in the schematic diagram in Fig. 3.

Variable	Definition
m_1	Combined mass of actuators, platform, and force-moment sensors.
m_2	Combined mass of load Ring, short I-beam, and long I-beam.
m_3	Combined mass of crossbeam and coil spring.
k_1	Combined lumped parameter stiffness of actuators (bending and compression)
k_2	Force-Moment sensors vertical stiffness.
k_3	Lumped parameter stiffness of crossbeam (bending)
k_4	Coil spring stiffness
c_1	Combined viscous damping coefficient from upper and lower ball joints and lead screw.
F_a	Combined force (vertical component) from linear actuators

Fig. 4 Definitions of Parameters in Schematic Diagram

Three differential equations were derived from the schematic diagram as shown in the following:

$$\begin{aligned} m_1 \ddot{x}_1 + c_1 \dot{x}_1 + k_1 x_1 + k_2 (x_1 - x_2) &= F_a \\ m_2 \ddot{x}_2 + k_2 (x_2 - x_1) + k_3 (x_2 - x_3) &= 0 \\ m_3 \ddot{x}_3 + k_3 (x_3 - x_2) + k_4 x_3 &= 0 \end{aligned}$$

Its state space representation can be shown as:

$$\begin{bmatrix} m_1 & 0 & 0 \\ 0 & m_2 & 0 \\ 0 & 0 & m_3 \end{bmatrix} \begin{bmatrix} \ddot{x}_1 \\ \ddot{x}_2 \\ \ddot{x}_3 \end{bmatrix} + \begin{bmatrix} c_1 \\ 0 \\ 0 \end{bmatrix} \begin{bmatrix} \dot{x}_1 \\ \dot{x}_2 \\ \dot{x}_3 \end{bmatrix} + \begin{bmatrix} k_1 + k_2 & -k_2 & 0 \\ -k_2 & k_2 + k_3 & -k_3 \\ 0 & -k_3 & k_3 + k_4 \end{bmatrix} \begin{bmatrix} x_1 \\ x_2 \\ x_3 \end{bmatrix} = \begin{bmatrix} F_a \\ 0 \\ 0 \end{bmatrix}$$

Using the set of equations, a Simulink Diagram in MATLAB was constructed in Fig. 5.

III. CALCULATION OF STIFFNESS VALUES

The six "legs" of the Stewart Platform are called actuators since they contain an AC motor in each of the legs. When the coil spring at the top of the Stewart Platform is in contact with the ceiling structure, the distance between the lower ball joint center to the upper ball joint center of the actuator measures 4199.43 mm. The angle with respect to horizontal, θ , is 51.70° as shown in Fig. 6. The material of all the parts mentioned in this section is SAE 6150 Alloy Steel which has a Young's Modulus of 200 GPa.

A. Actuator Spring Constant in Axial Direction

The spring constant of the right portion in the actuator, called "top cylinder" is calculated as:

$$k_{Topcyl,comp} = \frac{EA}{L} = \frac{200 \times 10^9 \text{ Pa} \times \pi \times (0.0316 \text{ m})^2}{4 \times 0.0277 \text{ m}} = 5.66 \times 10^9 \text{ N/m}$$

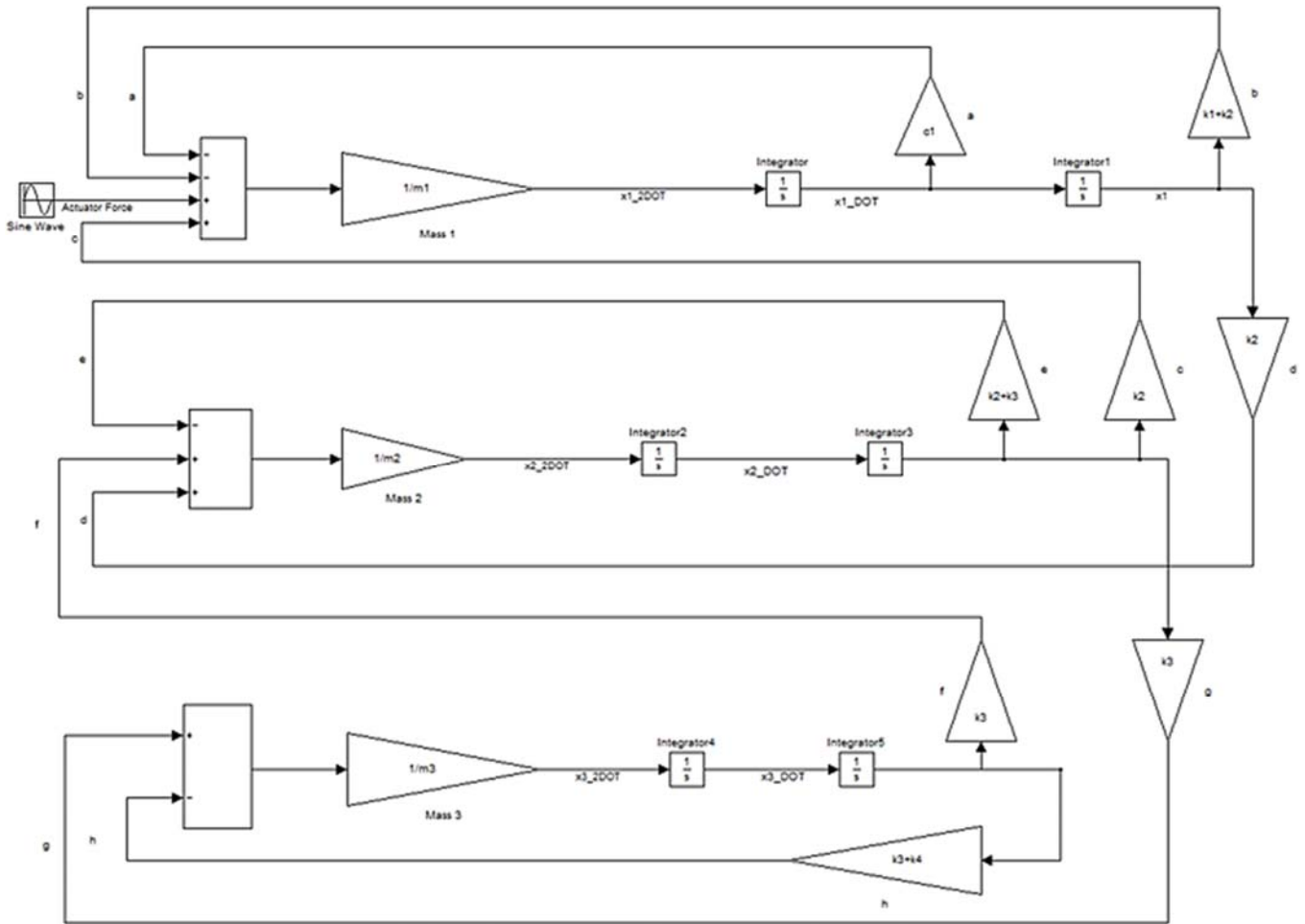


Fig. 5 Simulink Diagram of the Lumped Mass Model

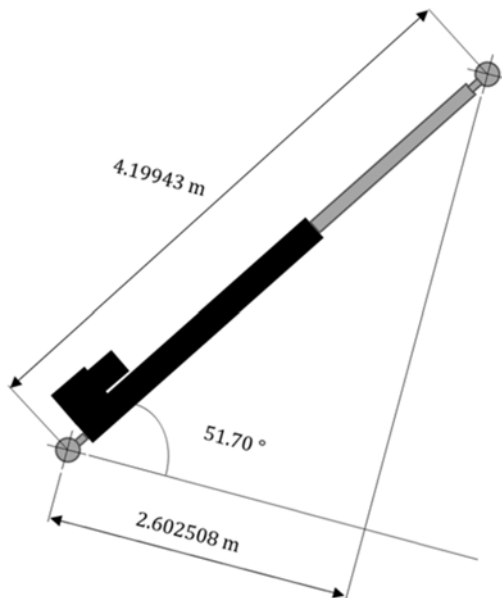


Fig. 6 Actuator Configuration

The shaft is a circular tube; thus, the spring constant can be calculated as:

$$k_{shaft,comp} = \frac{EA}{L} = \frac{200 \times 10^9 Pa \times \pi \times [(0.1016 m)^2 - (0.0762 m)^2]}{4 \times 2.064 m} = 3.44 \times 10^8 N/m$$

The spring constant of the lead screw was calculated using the outer diameter of the threads in the cross-sectional area:

$$k_{ls,comp} = \frac{EA}{L} = \frac{200 \times 10^9 Pa \times \pi \times (0.063 m)^2}{4 \times 0.0944 m} = 6.60 \times 10^9 N/m$$

The spring constant of the connecting cylinder for the ball joint and its housing is calculated as:

$$k_{Bottomcyl,comp} = \frac{EA}{L} = \frac{200 \times 10^9 Pa \times \pi \times (0.0316 m)^2}{4 \times 0.0277 m} = 5.66 \times 10^9 N/m$$

Several components in the actuator are considered as rigid, such as ball joints, nuts, etc. Their spring effects are neglected from the spring constant calculations. The four spring constants calculated in the actuator are connected in series; thus the equivalent lumped stiffness, k_{eq} , can be obtained by:

$$\frac{1}{k_{eq}} = \frac{1}{k_1} + \frac{1}{k_2} + \dots + \frac{1}{k_n}$$

Using the four spring constants obtained earlier, we yielded the equivalent spring constant along the actuator axis direction:

$$k_{eq,comp} = 2.93 \times 10^8 \frac{N}{m}$$

B. Actuator Spring Constant in Bending Direction

The lumped parameter stiffness of the cylinder in between the upper ball joint and the shaft is calculated as:

$$k_{TopCyl,bend} = \frac{12EI_z}{L^3}$$

$$I_z = \frac{\pi d^4}{64}$$

$$k_{TopCyl,bend} = \frac{12 \times 200 \times 10^9 Pa \times \pi \times (0.0316 m)^4}{64 \times (0.0277 m)^3} = 5.513 \times 10^9 \frac{N}{m}$$

The length of the shaft where it is hollow, no nut, is 2.035m.

$$k_{Shaft,bend} = \frac{12EI_z}{L^3}$$

$$I_z = \frac{1}{2} \pi (R_2^2 - R_1^2) (R_2^2 + R_1^2)$$

$$I_z = \frac{1}{2} \pi [(0.0508 m)^2 - (0.0381 m)^2] [(0.0508 m)^2 + (0.0381 m)^2]$$

$$I_z = 7.1511 \times 10^{-6} m^4$$

$$k_{Shaft,bend} = \frac{12 \times 200 \times 10^9 Pa \times (7.1511 \times 10^{-6} m^4)}{(2.035 m)^3} = 2.03653 \times 10^6 \frac{N}{m}$$

The section where the nut is inside the shaft can be approximated as a solid cylinder with the diameter of the shaft.

$$k_{NutShaft,bend} = \frac{12EI_z}{L^3}$$

$$I_z = \frac{\pi d^4}{64}$$

$$k_{NutShaft,bend} = \frac{12 \times 200 \times 10^9 Pa \times \pi \times (0.1016 m)^4}{64 \times (0.029 m)^3} = 5.147 \times 10^{11} \frac{N}{m}$$

The part where the nut is on the lead screw can also be approximated as a solid cylinder with diameter of the nut.

$$k_{LS/Nut,bend} = \frac{12EI_z}{L^3}$$

$$I_z = \frac{\pi d^4}{64}$$

$$k_{LS/Nut,bend} = \frac{12 \times 200 \times 10^9 Pa \times \pi \times (0.092 m)^4}{64 \times (0.089 m)^3} = 1.197188 \times 10^{10} \frac{N}{m}$$

The lead screw itself would have a lumped parameter stiffness as:

$$k_{LS,bend} = \frac{12EI_z}{L^3}$$

$$I_z = \frac{\pi d^4}{64}$$

$$k_{LS,bend} = \frac{12 \times 200 \times 10^9 Pa \times \pi \times (0.063 m)^4}{64 \times (1.477158 m)^3} = 5.75788 \times 10^5 \frac{N}{m}$$

The housing can be assumed as rigid.

The stiffness of the cylinder where it connects the housing to the lower sphere is the same as the upper cylinder:

$$k_{BottomCyl,bend} = \frac{12EI_z}{L^3}$$

$$I_z = \frac{\pi d^4}{64}$$

$$k_{BottomCyl,bend} = \frac{12 \times 200 \times 10^9 Pa \times \pi \times (0.0316 m)^4}{64 \times (0.0277 m)^3} = 5.513 \times 10^9 \frac{N}{m}$$

Since the components are connected in series, the equivalent bending spring constant for the actuator can also be calculated using series equation which yielded:

$$k_{eq,bend} = 4.48786 \times 10^5 \frac{N}{m}$$

C. Combined Actuator Spring Constant in Y-Direction

The springs can be separated into their y-components using the angle θ since the force is being applied vertically. Fig. 7 illustrates how the springs can be converted to their y-components.

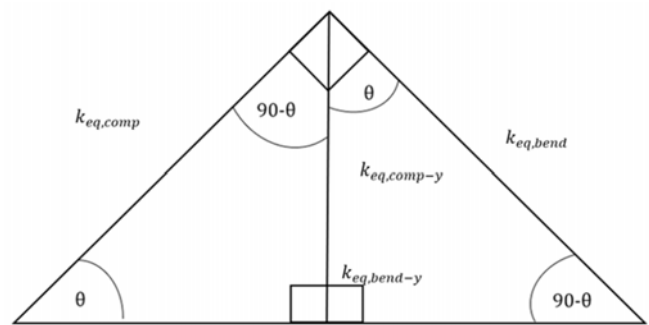


Fig. 7 Angle relation between bending and compression

The spring effect projects to the vertical, i.e., y direction, can be calculated as:

$$k_{eq,comp-y} = k_{eq,comp} \times \sin(\theta) = 2.9288 \times 10^8 \frac{N}{m} \times \sin(51.7^\circ)$$

$$k_{eq,comp-y} = 2.2984 \times 10^8 \frac{N}{m}$$

Likewise,

$$k_{eq,bend-y} = k_{eq,bend} \times \cos(\theta) = 4.48786 \times 10^5 \frac{N}{m} \times \cos(51.7^\circ)$$

$$k_{eq,bend-y} = 2.78148 \times 10^5 \frac{N}{m}$$

Finally, the spring effects in bending and compression can be combined in series to obtain the stiffness for a single actuator in y-direction as shown in Fig. 8.

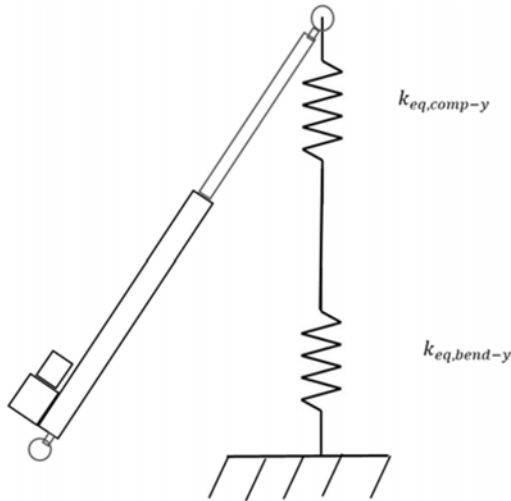


Fig. 8 Stiffness of an actuator in y-direction

$$\frac{1}{k_{1-single}} = \frac{1}{k_{eq,comp-y}} + \frac{1}{k_{eq,bend-y}}$$

$$\frac{1}{k_{1-single}} = \frac{1}{2.2984 \times 10^8 \frac{N}{m}} + \frac{1}{2.78148 \times 10^5 \frac{N}{m}}$$

$$k_{1-single} = 2.77812 \times 10^5 \frac{N}{m}$$

This is for one actuator, since all six actuators are parallel to each other and assumed to be equivalent, they can be combined by simply multiplying by a factor of six.

$$k_1 = k_{1-single} \times 6 = 2.77812 \times 10^5 \frac{N}{m} \times 6 = 1.667 \times 10^6 \frac{N}{m}$$

D. Spring Constant of Force Sensors

The force moment sensors from ATI are the Omega160 F/T Sensors. From the manufacturer's web page, the stiffness in the vertical axis is $1.2 \times 10^8 \frac{N}{m}$. Since the three F/T sensors are mounted on the same plane, parallel, they can be combined additively.

$$k_2 = 3 \times 1.2 \times 10^8 \frac{N}{m} = 3.6 \times 10^8 \frac{N}{m}$$

E. Spring Constant of Crossbeam

The material of the I-beam is AL 6061, thus $E = 69 \text{ GPa}$. For a bridge-like system (fixed-fixed beam), the stiffness is as follows:

$$k_t = \frac{192EI_z}{l^3}$$

For an I-Beam, segmenting the I-beam into three rectangles will be the first step in finding the moment of inertia. Next, to find the neutral axis (centroid of the beam):

$$\bar{y} = \frac{\Sigma Y_i A_i}{\Sigma A_i}$$

where Y_i is the center of mass of the individual rectangle and A_i is the area of the individual rectangle.

$$A_1 = b_1 \times h_1 = 3.332 \text{ in} \times 0.359 \text{ in} = 1.196188 \text{ in}^2$$

$$A_2 = b_2 \times h_2 = 0.232 \text{ in} \times 5.282 \text{ in} = 1.225424 \text{ in}^2$$

$$A_3 = b_3 \times h_3 = 3.332 \text{ in} \times 0.359 \text{ in} = 1.196188 \text{ in}^2$$

$$\Sigma A_i = 2 \times 1.196188 \text{ in}^2 + 1.225424 \text{ in}^2 = 3.6178 \text{ in}^2$$

$$Y_1 = h_3 + h_2 + \frac{h_1}{2} = 0.359 \text{ in} + 5.282 \text{ in} + \frac{0.359 \text{ in}}{2} = 5.8205 \text{ in}$$

$$Y_2 = h_3 + \frac{h_2}{2} = 0.359 \text{ in} + \frac{5.282 \text{ in}}{2} = 3 \text{ in}$$

$$Y_3 = \frac{h_3}{2} = \frac{0.359 \text{ in}}{2} = 0.1795 \text{ in}$$

$$\bar{y} = \frac{Y_1 A_1 + Y_2 A_2 + Y_3 A_3}{\Sigma A_i} = \frac{5.8205 \text{ in} \times 1.196188 \text{ in}^2 + 3 \text{ in} \times 1.225424 \text{ in}^2 + 0.1795 \text{ in} \times 1.196188 \text{ in}^2}{3.6178 \text{ in}^2} = 3 \text{ in}$$

$$\bar{y} = 3 \text{ in}$$

The parallel axis theorem states:

$$I_{total} = \Sigma(\bar{I}_i + A_i d_i^2)$$

where \bar{I}_i is the moment of inertia for each rectangle and d_i is the distance from the centroid of an individual rectangle to the centroid of the beam.

Next step is to calculate the moment of inertias for each rectangle,

$$\bar{I} = \frac{1}{12} b h^3$$

$$\bar{I}_1 = \frac{1}{12} b_1 h_1^3 = \frac{1}{12} 3.332 \text{ in} \times (0.359 \text{ in})^3 = 0.012847 \text{ in}^4$$

$$\bar{I}_2 = \frac{1}{12} b_2 h_2^3 = \frac{1}{12} 0.232 \text{ in} \times (5.282 \text{ in})^3 = 2.849062 \text{ in}^4$$

$$\bar{I}_3 = \frac{1}{12} b_3 h_3^3 = \frac{1}{12} 3.332 \text{ in} \times (0.359 \text{ in})^3 = 0.012847 \text{ in}^4$$

The distance in between the centroids is simply:

$$d_1 = |Y_1 - \bar{y}| = |5.8205 \text{ in} - 3 \text{ in}| = 2.8205 \text{ in}$$

$$d_2 = |Y_2 - \bar{y}| = |3 \text{ in} - 3 \text{ in}| = 0 \text{ in}$$

$$d_3 = |Y_3 - \bar{y}| = |0.1795 \text{ in} - 3 \text{ in}| = 2.8205 \text{ in}$$

$$I_{total} = \bar{I}_1 + A_1 d_1^2 + \bar{I}_2 + A_2 d_2^2 + \bar{I}_3 + A_3 d_3^2 = 0.012847 \text{ in}^4 + 1.196188 \text{ in}^2 \times (2.8205 \text{ in})^2 + 2.849062 \text{ in}^4 + 1.225424 \text{ in}^2 \times (0 \text{ in})^2 + 0.012847 \text{ in}^4 + 1.196188 \text{ in}^2 \times (2.8205 \text{ in})^2 = 21.9066 \text{ in}^4 = 9.1182 \times 10^{-6} \text{ m}^4$$

The length of the I-beam is 1.172 m.

$$k_t = \frac{192EI_z}{l^3} = \frac{192 \times 6.9 \times 10^{10} \text{ Pa} \times 9.1182 \times 10^{-6} \text{ m}^4}{(1.172 \text{ m})^3} = 7.5037 \times 10^7 \text{ N/m}$$

Since k_3 was defined as the crossbeam,

$$k_3 = 7.5037 \times 10^7 \text{ N/m}$$

F. Spring Constant of Coil Spring

The coil spring, which is an adjustable component of the system, for most cases the spring constant, is selected as:

$$k_4 = 50,787 \text{ N/m}$$

IV. MASS VALUES

Mass values were calculated by the CAD software system. After entering material density and component geometry, mass values were obtained in Fig. 9. Note that Mass 3 included effective mass of Coil Spring k_4 . The mass values of ATI sensors were given by its manufacturer.

Group	Name	Mass (kg)	Total (kg)
Mass 3	Crossbeam	7.3819146	$m_3 = m_{eff} = m_{crossbeam} + \frac{m_{coil spring}}{3} =$
	Coil Spring	4.92517	$m_3 = 9.023637933 \text{ kg}$
Mass 2	Long I-Beam	8.44277	$m_2 = 221.42487 \text{ kg}$
	Short I-Beam	3.5228	
	Load Ring	209.4593	
Mass 1	3 x ATI's	8.16	$m_1 = 2167.079 \text{ kg}$
	Platform	801.419	
	6 x Actuators	1357.5	

Fig. 9 Mass Values in Schematic Diagram

V. MOTOR TRANSFER FUNCTION

The electrical motor in each of the six actuators had unknown characteristics to us. A system identification process was used to obtain its input output relation, i.e., transfer function. Chirp tests allow the user to test a wide range of speed changes of a motor system [7], [8]. The input of our test, a chirp waveform, was a sinusoidal wave with a commanded torque within +/-10 Nm that increased in frequency over time.

Vector Fitting has since its first introduction in 1999 become a widely applied tool for fitting a rational model to frequency domain data [9]. The vectfit3.m function, a fast, relaxed vector fitting method, in MATLAB [10] was used to process the motor input/output data. The function computed a rational approximation from the input data in the frequency domain. The resulting model can be expressed in either pole-residue form or state-space form. The pole-residue form of the motor is shown in the following with the coefficients shown in Fig. 10.

$$T(s) = \frac{a_3 s^3 + a_2 s^2 + a_1 s + a_0}{(b_3 s^3 + b_2 s^2 + b_1 s + b_0)s}$$

Coefficient	Value
a_0	3.789479e+05
a_1	8.5989e+03
a_2	-17.6187
a_3	1.87467e-02
b_0	4.17849e+04
b_1	3.34462e+04
b_2	788.3805
b_3	1

Fig. 10 Transfer Function Coefficients

VI. CONCLUSIONS AND RECOMMENDATIONS

A hardware model of the Stewart Platform in a lab at NASA Johnson Space Center was developed. The task resulted in a one-directional dynamic model for the purpose of analyzing the up-and-down motions in docking operations. Detailed calculations of spring constants and masses were derived. A system identification process was used to obtain the characteristics of the motor used in the actuators. Damping coefficients in the system can vary due to changes of temperature, surface cleanliness, lubrication condition, force level, etc., and are very difficult to obtain from calculations. Experimental methods are recommended to obtain suitable damping coefficients. For the future computer simulation tasks, we will assume an initial damping coefficient at the ball joints. The actual value is to be determined through system validation via experimental data.

ACKNOWLEDGMENTS

The authors would like to thank Robert Zehentner and Daniel Erdberg of CACI, Cecil Shy and Mike Red at NASA JSC, and many other colleagues working at JSC for the research opportunities, sponsorship, and support.

REFERENCES

- [1] D. Stewart "A Platform with Six Degrees of Freedom." Proceedings of the Institution of Mechanical Engineers. 180 (1, No 15): 371-386, 1965-1966.
- [2] D.R. Riley, B.M. Jaguet, J.E. Pennington, et al, "Comparison of Results of Two Simulations Employing Full-size Visual-cue for Pilot-controlled Gemini-Agena Docking. NASA TND-3687, 1966:1-35.

- [3] U.S. Congress, Office of Technology Assessment. U.S. – Russian Cooperation in Space. OTA-ISS-618. U.S. Government Printing Office. 1995: 1-130.
- [4] C. Lange, & E. Martin. "Towards Docking Emulation Using Hardware in the Loop Simulation with Parallel Platform," Proceedings of the Workshop on Fundamental Issue and Future Directions for Parallel Mechanism and Manipulators, Quebec, Canada, 2002: 1-4.
- [5] J. Han, Q. Huang, & T. Chang, "Research on Space Docking HIL Simulation System Based on Stewart 6-DOF Motion System," Proceedings of the 7th JFPS International Symposium on Fluid Power, Toyama, Japan, September 2008.
- [6] J. Ueda, Y. Sadamoto, "A Measurement of the Effective Mass of Coil Springs." Journal of the Physical Society of Japan. 66 (2): 367-368, 1997.
- [7] W. Uddin, R. Mitra, T. Husain, & E. Ofori, "A Chirp PWM Scheme for Brushless DC Drives," IEEE Conference on Energy Congress and Exposition, September 2012.
- [8] H. Yang, S.B. Ryu, H.C. Lee, S.G. Lee, S.S. Yong, & J.H. Kim, "Implementation of DDS chirp signal generator on FPGA," International Conference on Information and Communication Technology Convergence, pp. 956-959, 2014.
- [9] B. Gustavsen and A. Semlyen, "Rational approximation of frequency domain responses by Vector Fitting," IEEE Trans. Power Delivery, Vol. 14, No. 3, pp. 1052-1061, July 1999.
- [10] B. Gustavsen, "User's Guide for vectfit3.m – Fast, Relaxed Vector Fitting for MATLAB," SINTEF Energy Research, Trondheim, Norway, 2008.